Digest Journal of Nanomaterials and Biostructures Vol. 8, No. 4, October – December 2013, p. 1621 - 1632

RETROGRESSION AND RE-AGING OF ALUMINUM ALLOYS (AA 7075) CONTAINING NICKEL

HAIDER T. NAEEM[a,b*], KAHTAN S. MOHAMMED[a]
[a]*School of Materials Engineering, University Malaysia Perils, Taman Muhibbah, 02600 Jejawi, Perlis, Malaysia*
[b]*Al-Muthana University, Samawa, Al-Muthana, Iraq*

In this study the effects of nickel additions in improving the mechanical properties and microstructure for high-strength aluminum alloys (AA7075) produced by semi-direct chill casting were investigated. Aluminum alloys were homogenized at different temperatures, aged at 120 °C for 24 h (T6), and retrogressed at 180 °C for 30 min and then re-aged at 120 °C for 24 h (RRA). The results of the microstructural analysis showed that adding nickel to aluminum alloy led to form nickel-rich dispersoid particles, such as Al_7Cu_4Ni, Al_4Ni_3, $Al_{75}Ni_{10}Fe_{15}$, Al_3Ni_2, and $Al_{50}Mg_{48}Ni_7$. These provided particles strengthening of dispersion and fine-grain that led to prevent the recrystallization besides restricted the grain growth. The mechanical properties of the alloys were improved by the strengthened dispersoid particles and precipitation of the matrix base alloy. The highest ultimate tensile strength and Vickers hardness of aluminum alloy containing nickel after the retrogression and re-aging treatment were about 400 MPa and 225 HV, respectively. Microstructure characterization of the alloys were carried out using optical microscopy (OM), scanning electron microscopy (SEM), energy dispersive X-ray (EDX) and X-ray diffraction (XRD).

(Received July 6, 2013; Accepted November 11, 2013)

Keywords: Aluminum alloys (7xxx); Trace element; Re-aging; Microstructural; Orowan strengthening

1. Introduction

Al-Zn-Mg-Cu aluminum alloys have been studied by many researchers because of their suitable properties and tremendous applications, especially in the aviation and aerospace industries [1].

High-strength aluminum alloys (7xxx) are popular because of their excellent properties, such as high tensile strength, excellent formability, and satisfactory corrosion resistance through heat treatments. The retrogression and re-aging (RRA) is considered one of the most important the heat treatments to produce materials with higher mechanical strength and stress corrosion than aging at T6 temper [2, 3]. The microstructural properties of aluminum–zinc–magnesium–copper alloys after the RRA treatment have been investigated. Typically, the eutectic structures of alloys consist of α-Al and $MgZn_2$. Several other phases such as *S*-Al_2CuMg, T-$Al_2Mg_3Zn_3$, and Al_2Cu are formed by solidifying aluminum alloys (Al-Zn-Mg-Cu) [4, 5]. The zinc–magnesium ratio significantly affects the formation of the $MgZn_2$ phase. High of zinc–magnesium ratio increases the formation other compounds of $MgZn_2$ that strengthen the alloys after heat treatments. Different nucleation agents, such as zirconium (Zr), titanium (Ti), boron (B), and scandium (Sc) have been used in aluminum alloys (7xxx); Ti coupled with B provides the finest microstructure for alloys [6,7]. Various studies have investigated the effect of nickel on the microstructure and mechanical properties of aluminum alloys. Compton et al. [8] found that adding nickel into pure aluminum forms Al_3Ni through eutectic reaction and increases alloy hardness. This intermetallic phase is also common in Al-Si-Ni alloys. Yang and Boyuk [9, 10] discovered that blending nickel into

*Corresponding author: haider_neem@yahoo.com .

aluminum–silicon alloys forms Al_3Ni in addition to Al_7Cu_4Ni and Al_9FeNi during solidification. For aluminum–silicon–nickel alloys, a nickel-rich dispersion phase insoluble at high temperature improves mechanical properties for applications in high temperatures [11–13]. Moreover, influence addition of nickel on the mechanical properties of Al-Zn-Mg-Cu alloys was investigated using numerous techniques such as; Ingot metallurgy (IM) and rapid solidification (RS).

Shen et al. and Wu et al. [14, 15] found that more semi-coherent and incoherent η′ and η phases in the microstructure of aluminum alloys Al-Zn-Mg-Cu-Ni produced by rapid solidification it's increased hardness after the aging. So a detailed understanding of the microstructural characteristics of Al-Zn-Mg-Cu containing Ni produced by semi-direct chill casting is still lacking. The purpose of this study aims to determine the effects of nickel additives on microstructural evolutions and mechanical properties of AA7075 aluminum alloys (produced by semi-direct chill casting) after aging and RRA.

2. Experimental procedures

2.1. Research Material

The present study was carried out on AA7075-O aluminum alloy slabs provided by ALCAN GLOBAL AEROSPACE. The slabs were 13 mm thick and 20 mm wide. Nickel of 99% purity as additives was provided by Merck KGaA. The nominal compositions of the studied alloys are listed in Table 1. The terms “Base alloy” and “Alloy A” refer to as received alloy and alloy with 0.1 wt. % Ni respectively. The chemical composition analysis was carried out using the arc-spark spectrometer (SPECTROMA).

Table 1: The chemical composition of studied alloys (in wt. %).

No.	Si	Fe	Cu	Mg	Cr	Ni	Zn	Ti	Al
Base alloy	0.066	0.24	1.8	2.87	0.18	-	6.68	0.03	balance
Alloy A	0.06	0.22	1.7	2.75	0.18	0.1	6.68	0.028	balance

Alloys were re-melted in a graphite crucible at 850°C (1123 K) in electrical resistance furnace (with accuracy of +/-5°C). The samples were produced by a semi−direct chilling (DC) casting process proceeded in iron steel mold of (150 *l* x 30 *w* x 20 *h*). The mold was preheated to 250°C prior to casting process. The casting speed about *150 mm/min*, water flow rate was about *45 l/min* and cooling rate of *–280°C /sec*. The alloys were inverted and remelted three times to ensure complete mixing. After the casting; homogenizing treatments conducted for alloys according to step No.1 in Table 2, followed by quenching in cold water immediately after each step of the homogenizing treatments. Thereafter ageing at T6 temper then the retrogression and re-aging (RRA) process their detailed in Table 2; quenching in cold water come after each treat.

Table 2: The homogenizing and heat treatment steps for alloys studied

No.	Type	Description of treatment
1	Homogenizing	450°C for 2 h+470°C for 24 h+480°C for ½ h
2	Ageing (T6)	120°C for 24 h
3	Retrogression and reaging (RRA)	120°C for 24 h + 180°C for ½h + 120°C for 24h

2.2. Microstructures Characterizations

The microstructures were analyzed by the optical microscopy (OM) using Olympus PMG3 optical microscope. The specimens were extracted from position of ½ height of the ingot, ground and polished according to ASTM E3-01. They were etched with Keller's reagent. The calculation of the average grain size and its analysis were carried out using the linear intercept method. In order to investigate effects of additives on the microstructure scanning electron microscopy (SEM) coupled energy dispersive X-ray (EDX) and X-ray diffraction analysis (XRD) were used.

2.3 Mechanical Testing

The Hv microhardness measurements were carried out on the specimens according to ASTM E92-82, "Mitutoyo DX256 series". Indentation force was set to 30N and 10 sec. dwelled time. To ensure cleanliness the surfaces of the samples were polished prior to Hv measurement. Each reading was an average of at least ten separate measurements taken randomly on the surface of the specimens. The highest and the lowest values of the ten reading were disregarded. The tensile test was carried out at ambient temperature on plate tensile specimens using INSTRON testing machine at a ram speed of 10mm/min., and a load of 500kN. The tensile test specimens were prepared according to ASTM B557M-02a. The tensile test was carried out at ambient temperature on plate tensile specimens using INSTRON testing machine at a ram speed of 10mm/min., and a load of 500kN. The tensile test specimens were prepared according to ASTM B557M-02a.

3. Results

Fig. 1(a) and 1(b) show the optical micrographs of as-quenched the base alloy and alloy A samples. These samples contained incipient dendrites of aluminum-rich solid solution and an interdendritic network of intermetallic compounds around the primary grains. Several fine equiaxed grains contained columnar grains between them.

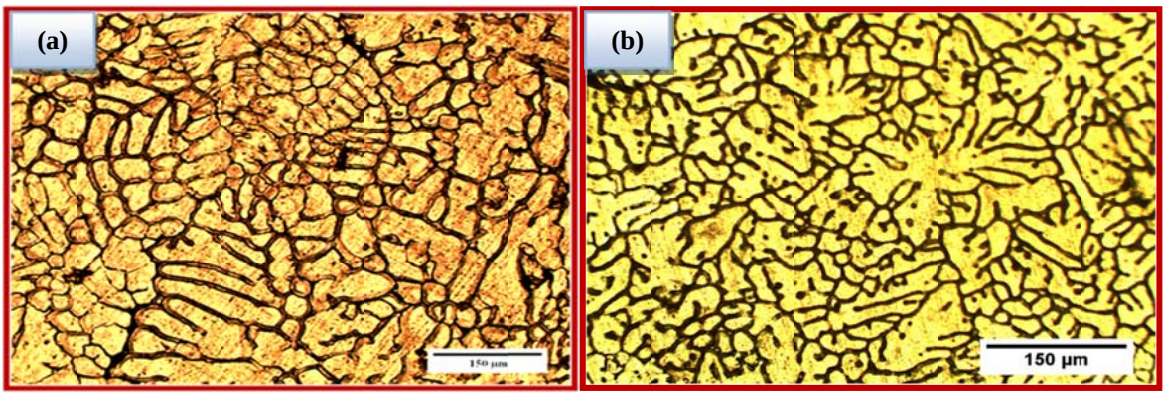

Fig. 1: Optical microstructures of as-quenched (a) base alloy and (b) alloy A samples

Semi-direct chill casting forms fine equiaxed grain structures all over the cross sections with an average grain size of about 45 and 39 µm for the base alloy and alloy A samples, respectively (Figs. 1a and 1b). Ying et al. [16] observed a grain size of about 121 µm for as-cast AA 7050 aluminum alloy. Average grain size is reduced by the nucleation rate during solidification in semi-direct chill casting [17]. The result of semi-direct chill casting in this study confirmed the efficiency of the technique in grain refinement and enhancement of mechanical properties. The grain size of as-quenched alloy A was refined by adding nickel to the aluminum alloy. Nickel acted as a nucleation agent on the grains, inhibiting columnar evolution, which usually starts from

the mold wall and forms appropriate sites for the nucleation of the first aluminum phases during solidification [18].

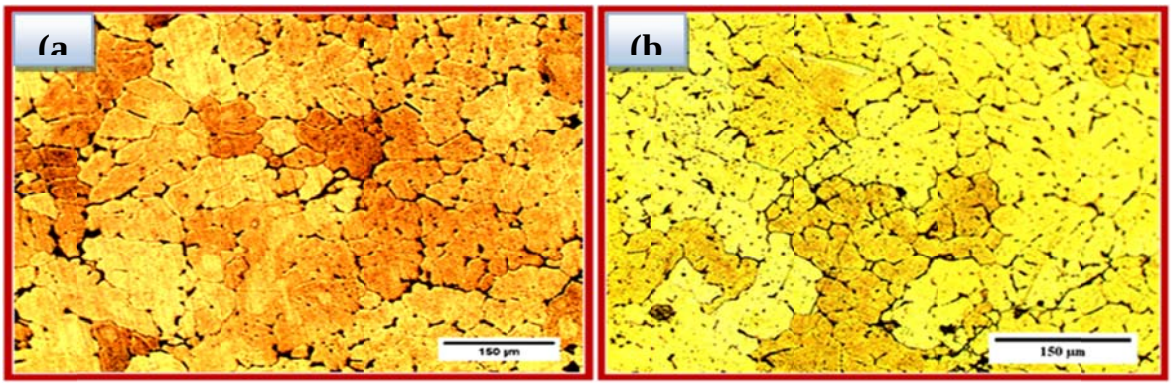

Fig. 2: Optical microstructures of (a) base alloy and (b) alloy A after T6 temper.

Fig. 2(a) and 2(b) show the optical micrographs of the alloy samples after promotive homogenizing and aging treatment at T6 temper. The average grain size was about 50 and 41 µm for the base alloy and alloy A samples, respectively. The volume fraction of the dendritic network structure was gradually reduced, and the residual phases became small and sparse because of the heat treatments.

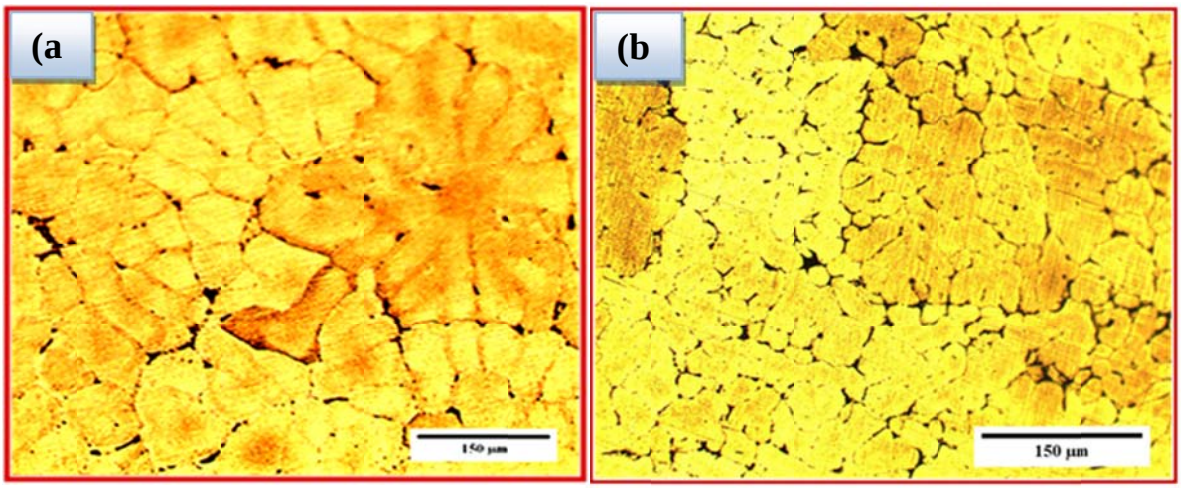

Fig. 3: Optical micrographs of (a) base alloy and (b) alloy A after RRA.

Fig. 3(a) and 3(b) show the optical micrographs of the base alloy and alloy A specimens after the RRA process. The average grain size of these alloys was about 53 and 43 µm, respectively. The grain size of the alloy A samples (Figs. 2 and 3b) was significantly reduced after the T6 temper and RRA treatment because of the interaction of matrix base alloy with nickel additives, which it's had higher density than the matrix base alloy and thus formed nucleation sites and increased the solidification rate.

With addition of nickel, eutectic reaction created dispersion compounds in the alloy. These compounds were formed because the solubility limits of the nickel were extended through a series of homogenization with heat treatments followed by quenching in cold water [19]. The newly formed compound of dispersed particles restricted recrystallization and grain growth in subsequent stages.

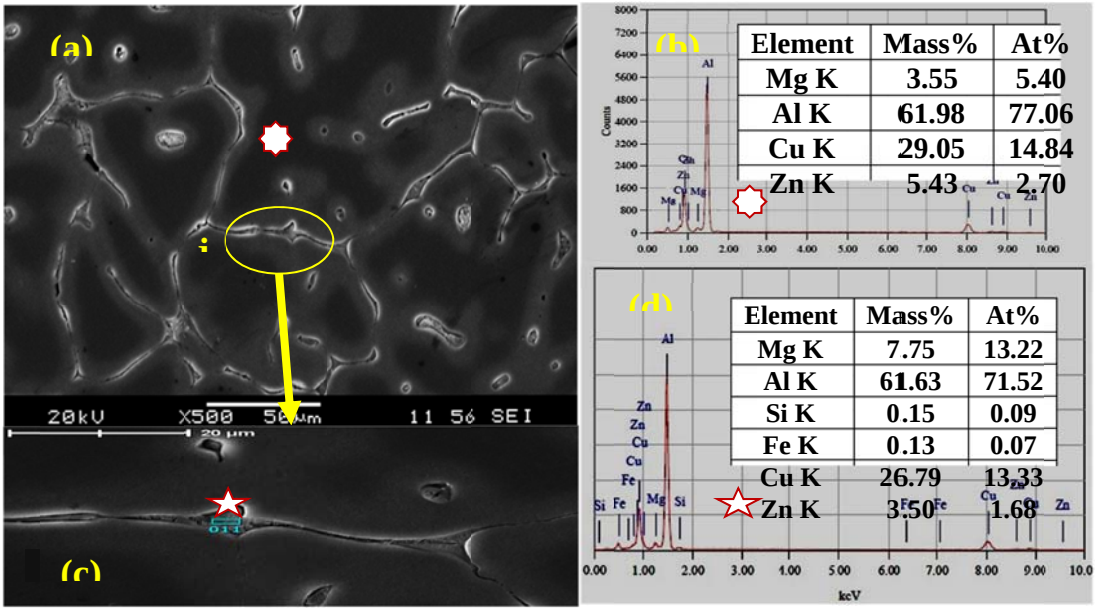

Fig. 4: (a) SEM and (b) EDX scan of as-quenched base alloy sample.

The scanning electron micrograph (SEM) in Fig. 4 shows the microstructure of the as-quenched base alloy sample. The dark areas indicate the primary solid solution and the bright areas indicate the non-equilibrium eutectic solid solution between grains; this eutectic solution had a lattice structure (Fig. 4c). Gray particles (encircled region (j)) were prevalent, suggesting stoichiometry similar to the T-($Al_2Mg_3Zn_3$) phase and the S-(Al_2CuMg) phase with Al-Cu-Fe (Fig. 4d). The labeled region in Fig. 4(a) represents the matrix of the base alloy. The energy-dispersive X-ray (EDX) scan in Fig. 4(b) reveals the chemical composition of the labeled region, in which the elements were similar to the T-($AlMg_4Zn_{11}$) and S-(Al_2CuMg) phases. Notably, the quantitative relation of Fe was not observed in this region. These results are consistent with those obtained by Fan [20], who found that aluminum alloys (7xxx) contain the T, S, and η phases with Al, Zn, Mg, and Cu.

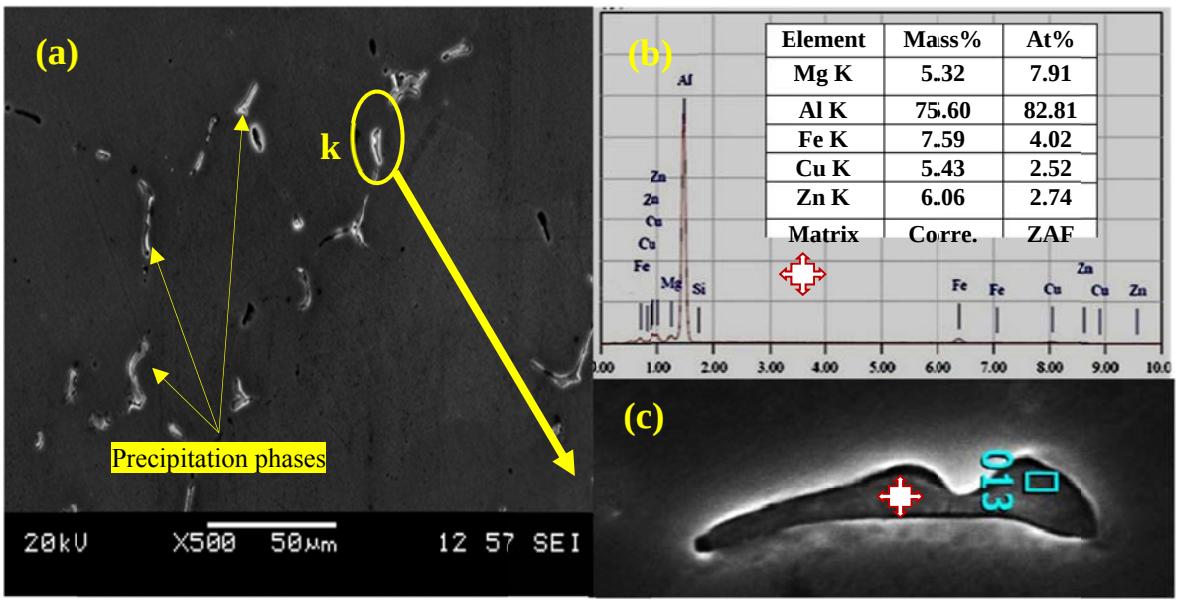

Fig. 5: (a) SEM and (b) EDX scan of base alloy sample after T6 temper.

The base alloy sample was homogenized under different temperatures conditions and aged at 120 °C for 24 h (T6). The SEM in Fig. 5(a) reveals the existence of precipitates (bright spots) with a script-like shape (encircled region (i), Fig. 5c). The EDX scan in Fig. 5(b) also reveals the chemical composition of the bright region. The stoichiometry of this labeled region was close to that of the T-$AlMg_4Zn_{11}$, S-Al_2CuMg, η′- Mg_2Zn_{11}, η-$MgZn_2$, and AlCuFe phases.

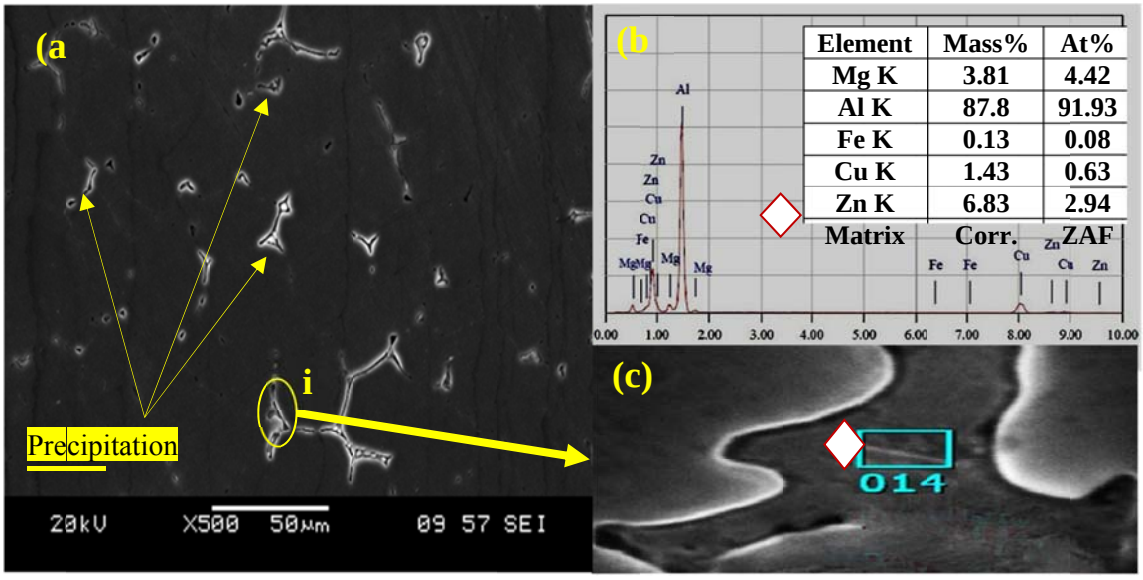

Fig. 6: (a) SEM and (b) EDX scan of base alloy sample after RRA heat treatment.

The SEM and EDX scan in Figs. 6(a) and 6(b) show the microstructure of the base alloy sample after RRA. The SEM reveals the existence of precipitates (bright spots) with a zag-like shape (encircled region (i), Fig. 6c). The EDX scan of the labeled region indicates that these bright spots exhibit stoichiometry close to that of T-$AlMg_4Zn_{11}$, S-Al_2CuMg, η-$MgZn_2$, η′-Mg_2Zn_{11}, and AlCuFe compounds (Fig. 6b).

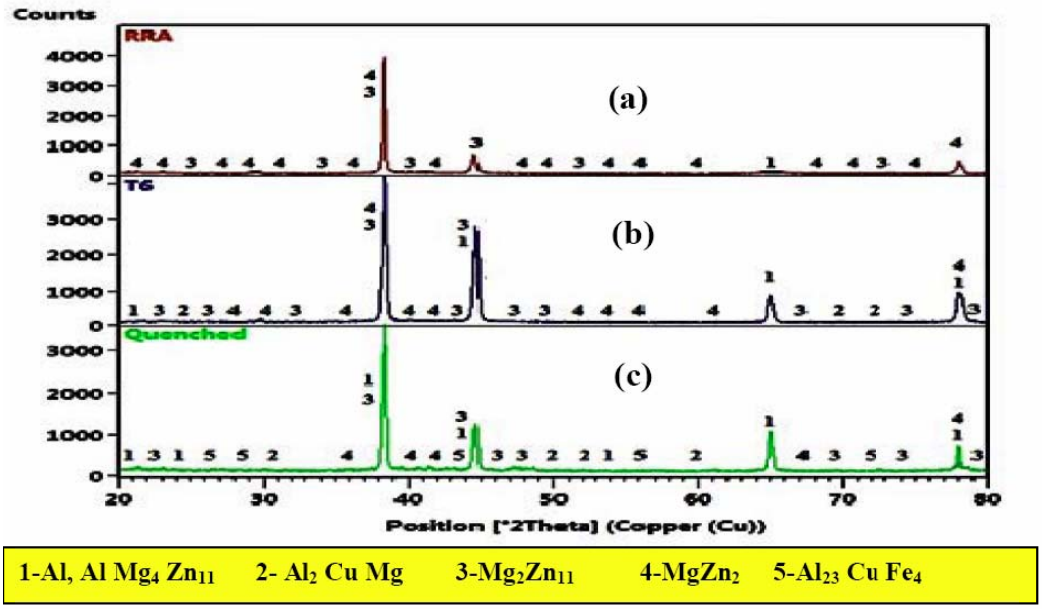

Fig. 7: XRD plots of base alloy as quenched, after T6 heat treatment, and after RRA.

Fig. 7 shows the different X-ray diffraction (XRD) patterns of the base alloy after quenching, T6 temper , and the RRA treatment. The as-quenched base alloy (c) was primarily composed of α-(Al), and the secondary phases were T-$AlMg_4Zn_{11}$, S-Al_2CuMg, η- $MgZn_2$, η′-Mg_2Zn_{11}, and $Al_{23}CuFe_4$, consistent with [20]. The generally accepted precipitation sequences for 7000 series aluminum alloys are as follows: [21-24]: supersaturated solid solution → coherent stable Guinier–Preston (GP) zones→ semi-coherent intermediate η′(Mg_2Zn_{11}) phase→ incoherent stable η($MgZn_2$) or T($AlMg_4Zn_{11}$) phase. Metastable η′phase was the primary precipitation hardening phase of these alloys. The primary precipitations in the matrix were the GP zones and η′(Mg_2Zn_{11}) phase after aging at 120 °C for 24 h.

The XRD plots in Fig. 7(b); shows that after T6 temper, the base alloy sample exhibited more significant η-$MgZn_2$ and η′-Mg_2Zn_{11} phases, which dissolved during homogenization and then precipitated during aging at T6. No obvious diffraction peak was observed in the $Al_{23}CuFe_4$ phase.

The different X-ray diffraction (XRD) findings for the sample after the RRA process (Fig. 7a) indicated high-intensity diffraction peaks in the $MgZn_2$ and Mg_2Zn_{11} phases. The primary precipitation phases in the matrix (the fine and dispersive GP zone and η′ phase) underwent the RRA treatment after its step first (120°C for 24 h) aging. During retrogression, the GP zones dissolved into the η′(Mg_2Zn_{11}) or η-$MgZn_2$ phases. With prolonged retrogression, the undissolved GP zones transformed into the η′ phase and thus formed numerous GP zones and η′ phases that were dissolved in the early stages of another round of retrogression [25, 26]. Finally, abundant nuclei that promote the re-precipitation of the GP zones and η′ phase in the re-aging step were mounted according to the XRD results. The XRD analysis results were consistent with the EDX results.

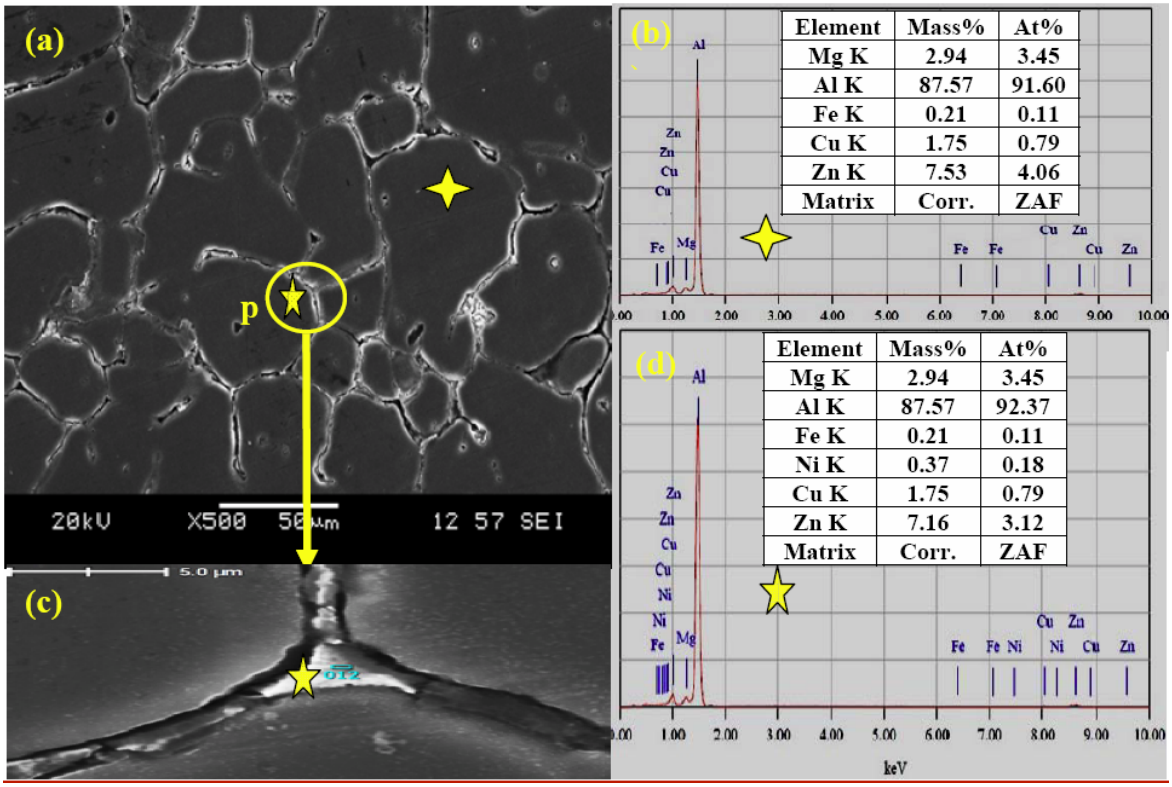

Fig. 8: (a) SEM and (b) EDX analysis of as-quenched alloy A sample.

The SEM in Fig. 8 (a) shows the microstructure of the as-quenched alloy A sample. The dark areas denote the primary solid solution as indicated in the matrix of the labeled region; the EDX scan points reveal chemical composition close to the T-$Al_5Mg_{11}Zn_4$, S-Al_2CuMg, η-$MgZn_2$,

η′-Mg_2Zn_{11}, and AlCuFe phases (Fig. 8b). The bright areas denote the non-equilibrium solidification eutectic system between grains (Fig. 8c). Gray particles were observed (encircled region (p), Fig. 8d), revealing stoichiometry close to the T-$Al_5Mg_{11}Zn_4$, S-Al_2CuMg, η-$MgZn_2$, η′-Mg_2Zn_{11}, γ-Al-Cu-Ni, and Al-Ni-Fe phases.

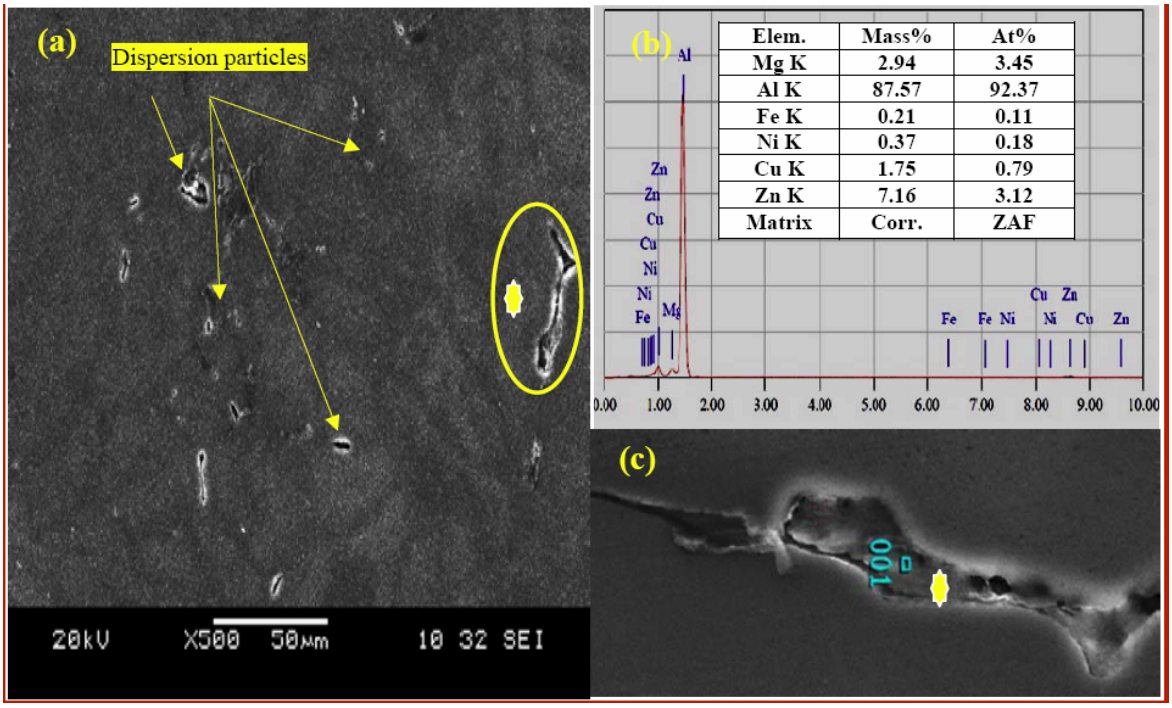

Elem.	Mass%	At%
Mg K	2.94	3.45
Al K	87.57	92.37
Fe K	0.21	0.11
Ni K	0.37	0.18
Cu K	1.75	0.79
Zn K	7.16	3.12
Matrix	Corr.	ZAF

Fig. 9: (a) SEM and (b) EDX analysis of alloy A sample after T6 temper.

Fig. 9(a) shows an SEM of the alloy A sample after T6 temper. The encircled region shows a bacillary shape (Fig. 9c). Figure 9(b) reveals chemical composition close to the T-$Al_5Mg_{11}Zn_4$, S-Al_2CuMg, Al_7Cu_4Ni, $Al_{50}Mg_{48}Ni_7$, Al_4Ni_3, Al_3Ni_2, $MgZn_2$, and Mg_2Zn_{11} phases. Figure 9(a) shows the prevalence of Ni-rich dispersion particles.

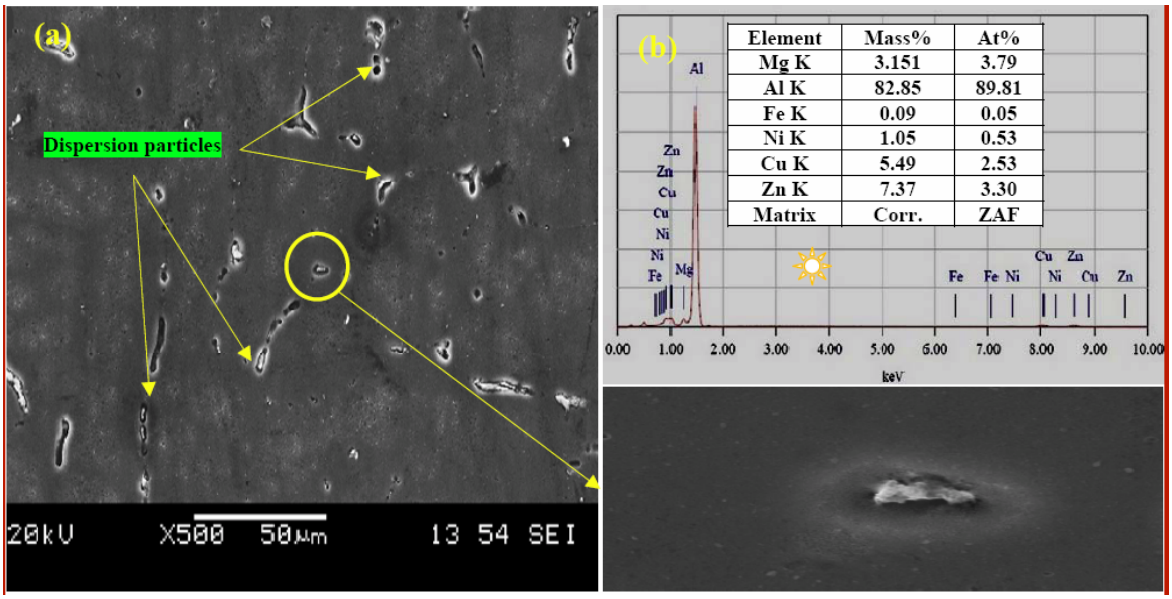

Element	Mass%	At%
Mg K	3.151	3.79
Al K	82.85	89.81
Fe K	0.09	0.05
Ni K	1.05	0.53
Cu K	5.49	2.53
Zn K	7.37	3.30
Matrix	Corr.	ZAF

Fig. 10: (a) SEM and (b) EDX analysis of alloy A sample after RRA.

Figure 10 shows the microstructure of the alloy A sample after the RRA process. The bright areas denote newly formed phases in addition to the dispersion particles. Figure 10(a) shows the numerous dispersion particles (see Fig. 10c for highly magnified SEM). Figure 10(b) reveals similar stoichiometry to that of Al_4Ni_3, Al_3Ni_2, $Al_{50}Mg_{48}Ni_7$, T-$Al_5Mg_{11}Zn_4$, S-Al_2CuMg, Al_7Cu_4Ni, $MgZn_2$, and Mg_2Zn_{11}. During RRA, the secondary phase particles were further dissolved into the matrix, and the solubility limit of the nickel additives can be extended with dual solution treatment, consistent with Yuan et al. [25].

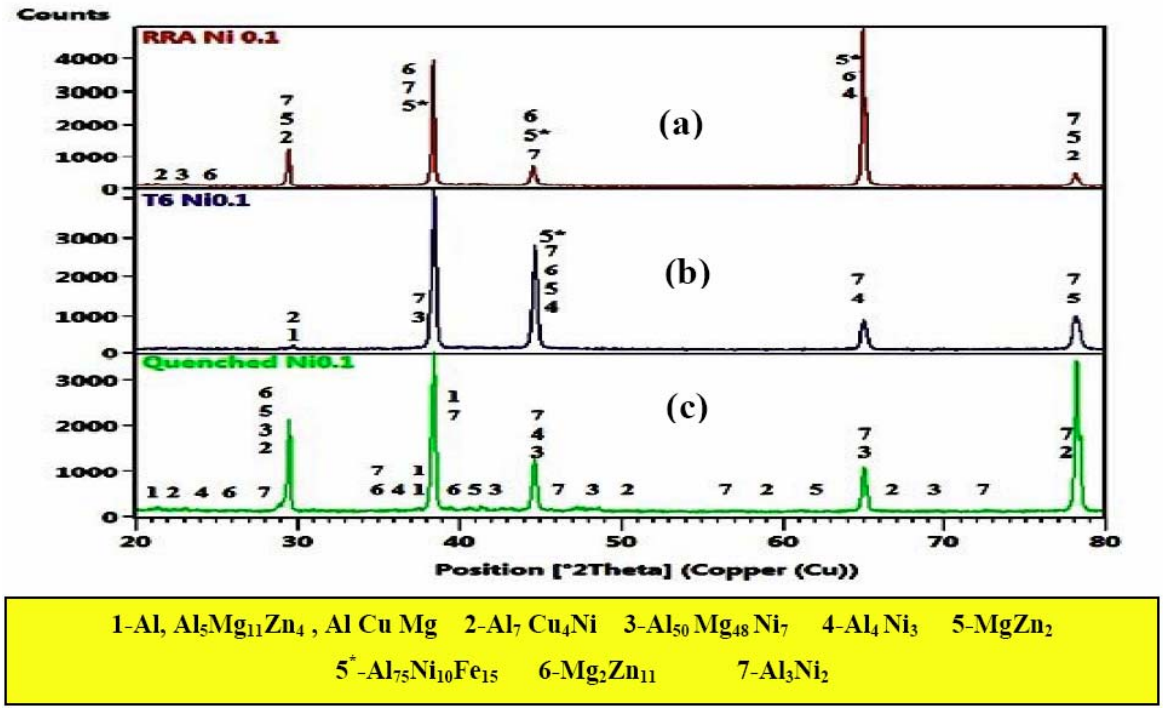

Fig. 11: XRD plots for alloy A after quenching, T6 heat treatment, and RRA.

The XRD analysis results for the alloy A samples are shown in Figs. 11(a)–11(c) (RRA, T6, and as-quenched, respectively). The patterns of the as-quenched alloy A sample confirm that the primary eutectic system mainly consisted of α(Al), solid solution, and intermetallic compounds (i.e., T-$Al_5Mg_{11}Zn_4$, S-Al_2CuMg, Al_7Cu_4Ni, $Al_{50}Mg_{48}Ni_7$, Mg_2Zn, Mg_2Zn_{11}, Al_4Ni_3, and Al_3Ni_2). The solubility limits of nickel can be extended to form a supersaturated solid solution with the aluminum matrix produced by chill casting and thus form nickel dispersion particles within the aluminum alloy [26]. This result was confirmed by the SEM/EDX and XRD results. Figure 11(b) shows the XRD plots for the alloy A sample after T6 temper and indicates the existence of the $Al_{75}Ni_{10}Fe_{15}$ phase in addition to the phases in the as-quenched sample ($Al_{50}Mg_{48}Ni_7$, Mg_2Zn, Mg_2Zn_{11}, Al_4Ni_3, and Al_3Ni_2). These dispersive phases had high peaks because of the intensive dissolution of the alloying elements with the nickel additives produced by the homogenization and subsequent heat treatments.

On the other hand, Li et al. [27] found that adding nickel to aluminum alloys Al-Zn-Mg suppresses the formation of the $MgZn_2$ phase in the matrix. These findings contradict the present results according to EDX and XRD analysis (i.e., numerous $MgZn_2$ phases).

Figure 11(a) shows the XRD plots for the alloy A sample after the RRA treatments. The intensity of the diffraction peaks of phases Al_4Ni_3, $Al_{75}Ni_{10}Fe_{15}$, Al_3Ni_2, $Al_{50}Mg_{48}Ni_7$, $MgZn_2$, and Mg_2Zn_{11} increased this because the effects of steps the retrogression and reaging as is detailed above (Fig.10).

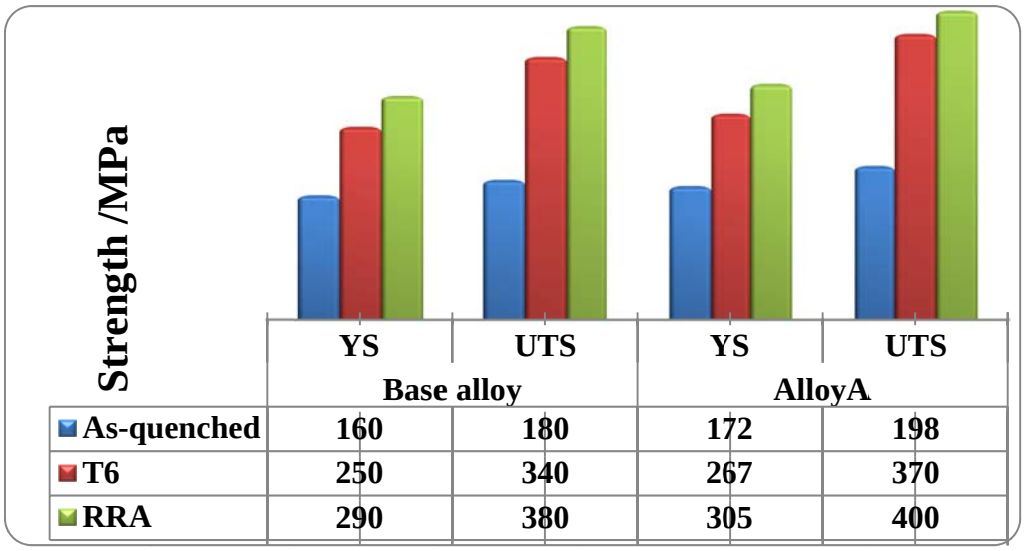

Fig. 12: Variations in tensile strength of alloy specimens before and after different heat treatment conditions.

Fig. 12 indicates the strength of two alloys under different conditions. Treating the two alloys with the T6 temper and RRA process yielded maximum gains of 160 and 200 MPa (T6) and 172 and 202 MPa (RRA) in ultimate tensile strength (UTS). The variation in the UTS of the as-quenched alloy samples after T6 temper and RRA was due to grain refinement and the evolution of interdendritic networks by the heat treatments (Fig.1).

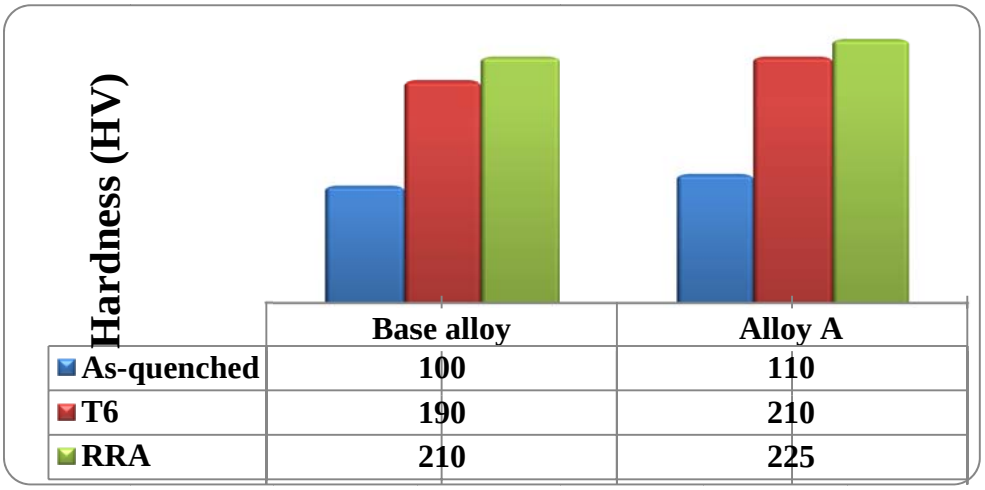

Fig. 13 indicates the variations in the Vickers hardness of the alloy specimens under different conditions.

Maximum gains of 100 and 110 HV (base alloy) and 100 and 115 HV (alloy A) in Vickers hardness were obtained.

4. Discussion

The results indicated that the yield strength (YS), UTS, and Vickers hardness of both the base alloy and alloy A substantially improved after T6 temper and RRA (in addition to the

addition of nickel additives in alloy A). The strengthening mechanism of aging at T6 (120 °C for 24 h) for the base alloy is attributed to precipitation hardening; that is, the effects of the GP zones were consistent with the nano-sized η′ metastable precipitates. These precipitates act as pinning points that impede dislocation [23–26]. The XRD and EDX results revealed the existence of η and η′ phases. The YS and UTS of the base alloy sample after RRA significantly improved compared with those of the T6 temper specimens. This improvement is attributed to the partial dissolution of the pre-existing GP zones and η′ phase. The GP zones can act as nucleation sites for η′ particles, and the remaining η′ phase constantly grew during RRA. After the RRA, the solute atoms dissolved in the matrix precipitated again and produced smaller GP zones and η′ phase. Therefore, η($MgZn_2$) and η′(Mg_2Zn_{11}) phases were more significantly augmented by RRA than by the T6 process. The strengthening mechanisms for nickel microalloying additions to Al-Zn- Mg-Cu alloys can primarily be classified into precipitation strengthening by the alloying element for the base alloy and dispersion and fine-grain strengthening by Ni-rich dispersoid particles. Precipitation was strengthened by the heat treatment. Dispersion can be described as dislocations inhibited by Ni dispersoid particles in the slipping planes. The dispersoid phase particles were looped, bypassed, and/or sheared by dislocation through the Orowan mechanism. The stress required to move a dislocation around a particle is YS, which is increased by dispersion strengthening. Aside from the fine-grain strengthening, Ni-rich dispersoid particles restrict recrystallization and inhibit grain growth (Figs. 2 and 3b). This outcome increases YS.

5. Conclusions

The microstructure of the base alloy contained $Al_5Mg_{11}Zn_4$, Al_2CuMg, Mg_2Zn_{11}, and $MgZn_2$ phases. Adding nickel into the base alloy formed new dispersion particles, such as Al_7Cu_4Ni, Al_4Ni_3, $Al_{75}Ni_{10}Fe_{15}$, Al_3Ni_2, and $Al_{50}Mg_{48}Ni_7$ particles.

RRA improved the YS of the base alloy more significantly than the T6 temper and significantly increased UTS (i.e., 380 MPa; Vickers hardness = 210).

RRA increased the YS of alloy A more significantly than it did the YS of the base alloy.

The YS of alloy A was increased by the dispersion phase particles (Al_7Cu_4Ni, Al_4Ni_3, $Al_{75}Ni_{10}Fe_{15}$, Al_3Ni_2, and $Al_{50}Mg_{48}Ni_7$), which restricted recrystallization and grain growth.

The strengthening mechanisms for the two alloys were precipitation related to the alloying elements for the base alloy and the dispersion addition to the fine grains by the Ni-rich dispersoid particles.

Acknowledgements

This work is supported under the grant No. 9001-00338 of the Universiti Malaysia Perlis (UniMAP). The authors gratefully acknowledge the outstanding support provided by the technicians of the work shop of Materials Engineering School, UniMAP.

References

[1] K.S. GHOSH, N. GAO , Trans. Non ferr. Met. Soc. China **21**, 1199 (2011).
[2] F. Viana , A.M.P. Pinto , H.M.C. Santos, A.B. Lopes , journal of Mat. Processing Tech. **92-93,** 54 (1999).
[3] A.F. Oliveira, Jr., M.C. de Barros, K.R. Cardoso, D.N. Travessa, Mat. Sci. and Eng. A **379,** 321 (2004).
[4] Seong Taek Lim, II Sang Eun and Soo Woo Nam, Mat.Tran.**44**(1), 181 (2003).
[5] A. K. Mukhopadhyay, Trans. Ind. Ins. Metal. **62**, 113 (2009).
[6] K. T. Kashyap, T. Chandrashekar, Bull. Mater. Sci. **24**, 345 (2001).
[7] H. Yongdong, Z. Xinming, C. Zhiqiang, Rare Metal Mat. Eng. **39**, 1135 (2010).
[8] D. N. Compton, L. A. Cornish, M. J. Witcomp, J. Alloy.Compd. **317-318,** 372 (2001).

[9] Yang Yang, Kuilong Yu, Yunguo Li , Degang Zhao, Xiangfa Liu, Mat. And Design **33**, 220 (2012).
[10] U. Boyuk, S. Engin, N. Marasli, Mater. Charact. **62**, 844 (2011).
[11] N. A. Belov, D. G. Eskin, N. N. Avxentieva, Acta Mater. **53**, 4709 (2005).
[12] Y. Yang, Y. Li, W. Wu, D. Zhao, X. Liu, Mat. Sci. Eng. A. **528**, 5723 (2011).
[13] H. A. Ammar, C. Moreau, A. M. Samuel, F. H. Samuel, H. W. Doty, Mat. Sci. Eng.A. **489**, 426 (2008).
[14] J. Shen, R. Liu, Y. Liu, Z. Jiang, Q. Li, J. Mater. Sci. **32**, 829 (1997).
[15] Y. Wu, F. H. Froes, C. Li, A. Alvarez, Metall. Mater. Trans. A. **30**, 1017 (1999).
[16] Ying Deng, Zhimin Yin, Fuguan Cong, Intermetallics **26**, 114 (2012).
[17] A.L. Greer, Grain Refinement Of Aluminum Alloys , TMS (2004) .
[18] O. P. Gbenebor , M. Abdulwahab , O.S.I. Fayomi, Influnce Of Inoculant Addition And Cooling Medium On The Mechanical Properties Of Aa 6063-Type Al-Mg-Si Alloy, Chalcogenide Letters.
[19] O.S.I. Fayomi, O.P.Gbenebor, M. Abdulwahab, C.A.Bolu, A.P.I. Popoola, "Structural Modification, Strengthening Mechanism and Electrochemical Assessment of the Enhanced Condition AA 6063-type Al-Mg-Si Alloys" Chalcogenide Letters, **16**, 059 (2013).
[20] Fan Xi-Gang, Jiang Da-Ming, Meng Qing –Chang, Trans. Nonferrous Met. Soc. China **16,** 577 (2006).
[21] Peng Guo-Sheng, Chen Kang-Hua, Chen Song-Yi, Fang Hua-Chan, Trans. Nonferrous Met. Soc. China **22**, 803 (2012).
[22] Li Xiwu , Xiong Baiqing, Zhang Yongan, Hua Cheng, Wang Feng, Zhu BaoHong & Liu HongWei, Trans. Nonferrous Met.Soc. China **16,** 1163 (2006).
[23] Li Guo-Feng , Zhang Xin-Ming , Li Peng-Hui , You Jiang-Hai, Trans.Nonferrous Met. Soc. China **20,** 935 (2010). TRANSACTIONS A,vol30A, 1999-1017.
[24] Robert J.Flynn, J.S.Robinson, Journal of materials processing Technology **153-154,** 674 (2004) .
[25] Wuhua Yuan, Jian Zhang , Chenchen Zhang , Zhenhua Chen , Journal of Materials Processing Technology **209**, 3251 (2009).
[26] I.J.Polmear, Light Alloys from traditional alloys to nanocrystals, Australia, Elsevier (2006).
[27] L. Li, et al., Trans. Nonferrous Met. Soc. China. **16**, 532 (2006).